Hindawi
International Journal of Antennas and Propagation
Volume 2022, Article ID 3067061, 11 pages
https://doi.org/10.1155/2022/3067061

Research Article

Ka-Band Single-Layer High-Efficiency Circular Aperture Microstrip Array Antenna

Shi-Shan Qi, Jun-Jie Zhao, and Wen Wu

Ministerial Key Laboratory of JGMT, Nanjing University of Science and Technology, Nanjing 210094, China

Correspondence should be addressed to Shi-Shan Qi; qishishan@gmail.com

Received 18 March 2022; Revised 24 June 2022; Accepted 6 September 2022; Published 29 September 2022

Academic Editor: Seong-Youp Suh

Based on microstrip antenna technology, a compact single-layer circular aperture array is proposed in this paper. The proposed method is suitable for designing large-scale and high-efficiency patch array in Ka band. By using the high-impedance characteristic of the coupled microstrip line, a novel multi-stage feeding network that can realize large power division ratio is proposed, and its structure is center-symmetrical and is fed through a coaxial probe at the center. The parallel branch of the multi-stage divider is connected to the row array, and the array elements can obtain uniform excitation through the design of the division ratio of each stage. A 256-element patch array operating at 35 GHz is proposed, the length and width of the antenna unit are 2.74 mm and 3 mm, respectively, the horizontal spacing between the array elements is $0.742\lambda_0$, the vertical spacing varies from $0.677\lambda_0$ to $0.737\lambda_0$, and the radius of the proposed array is 60 mm ($7\lambda_0$ at 35 GHz). At the end, a prototype is fabricated and measured, the measured results show that the maximum gain is 29.5 dBi at 35 GHz, which correspond to the radiation efficiency and aperture efficiency of 61.66% and 46.07%, respectively, and the results show that the proposed antenna achieves high efficiency in Ka band, which verifies the correctness of the design. The proposed array antenna is compact in structure and only needs single-layer design, which can achieve high efficiency and low in manufacture cost, which is an excellent candidate for millimeter-wave large-scale array application.

1. Introduction

Due to the characteristics of available spectrum resources and small size, Ka-band wireless systems are widely used in millimeter-wave applications. To improve system performance and reduce costs, a low-cost, low-profile, and high-efficiency antenna is commonly required for such systems [1]. However, conventional planar antennas are difficult to achieve high efficiency due to their large losses in millimeter waveband. Therefore, in order to obtain higher efficiency, most of the reported millimeter-wave antennas are in the form of non-planar antennas, such as metal waveguides, to achieve high gain by reducing high-frequency loss, but these antennas usually have the disadvantages of high profile and high cost, which is difficult to meet the needs of many millimeter-wave applications. Therefore, the low-cost low-profile antenna with high efficiency in millimeter-wave band has important research and application values.

As a classic planar antenna, microstrip antenna is widely used with the advantages of low profile and low cost, and the parallel-fed structure is often used in the design of microstrip array antennas [2, 3], which can make the array obtain a wide bandwidth, but it introduces great transmission loss, and the loss will become larger as the array scale increases. Using the substrate-integrated waveguide (SIW) or printed ridge gap waveguide (PRGW) technology to design the feeding network can greatly reduce path loss [4, 5]. For example, a high efficiency of 49.5% was obtained by feeding the slot antenna array through a PRBG unequal power divider in [4], and 41.6% efficiency was obtained by using SIW structure to excite a cavity-backed microstrip antenna in [6], and this design approach can improve antenna efficiency, but it requires double-layer or even multi-layer structure, which increases the manufacturing cost. Compared with parallel-fed structure, the microstrip array with the series-fed structure has lower high-frequency loss [7, 8].

In [8], 7 subarrays in series structure are excited by 6-branch edge parallel power dividers, and parasitic patches are added on the upper layer to enhance the bandwidth; although this method can reduce some transmission losses, the existence of the edge parallel power divider will occupy part of the antenna aperture, which will result in the loss of aperture efficiency. In order to realize the single-layer series-fed structure, a method of introducing short stubs arranged periodically with a waveguide wavelength as a period on the microstrip line is proposed in [9], but this design is not suitable for large-scale arrays. The gap waveguide structure is often used in millimeter-wave antennas [10, 11]; compared with the microstrip structure, the waveguide structure has lower loss and higher efficiency in millimeter-wave band; however, this structure also requires double-layer or even multi-layer, which leads to its disadvantages of complex structure and higher manufacture cost.

Although there have been many reports on planar antennas in millimeter-wave band, there are few reported antenna arrays that can achieve both high efficiency and single-layer. In addition, most of the reported arrays are designed with a rectangular aperture, which is not suitable for some special needs of circular aperture applications.

In this paper, a single-layer circular aperture high-efficiency microstrip array antenna that works in *Ka* band is presented. By using the high-impedance characteristic of the coupled microstrip line, a novel multi-stage feeding network that can realize large division ratio is proposed, which can excite each array element with equal amplitude. The proposed antenna guarantees high efficiency through two aspects. On the one hand, the feeding network has a short path and a compact structure, which reduces the transmission loss of the feeding path. On the other hand, through the design of the division ratio of the multi-stage divider, ensures that the radiation amplitude of each array element is uniform. Therefore, higher radiation efficiency can be obtained. In addition, the array elements are compactly arranged in the aperture, the feeding network does not occupy additional space, and the antenna aperture is well utilized, ensuring that the array can achieve high aperture efficiency. The proposed array only needs single-layer structure, which is easy to manufacture and low in cost. At the end, a prototype is fabricated and measured to verify the validity of the design.

2. Antenna Configuration and Design

The configuration of the proposed antenna is shown in Figure 1. The antenna array with 256 elements is printed on Rogers 5880 substrate ($\varepsilon_r = 2.2$) with height of 0.254 mm and radius of 60 mm ($7\lambda_0$ at 35 GHz). The feeding point is located at the center of the array and fed by a back inserted coaxial probe. The central feeding network is composed of multi-stage one-to-three dividers, the energy is transmitted to each row array through the parallel branch of the divider at each stage, and the energy is further divided to each series patch. Each array element in the array can be excited with equal amplitude by controlling the division ratio of the feeding network at each stage, and the excitation obtained by the elements can be in the same phase by controlling the distance between the elements. Therefore, through the careful design of the feeding network, each element in the array can be excited with equal amplitude and in-phase.

2.1. Design of High-Impedance Line. In order to realize high efficiency and high gain in millimeter-wave band, the series-fed structure is usually chosen instead of the parallel-fed structure to reduce the transmission loss of the feeding line; at the same time, it should be ensured that the radiation amplitude of each array element is uniform. However, it is difficult to realize a large division ratio for traditional microstrip divider, and this is due to the difficulty in realizing flexible impedance characteristics of traditional microstrip line. The width of microstrip line will be too thin to manufacture when the characteristic impedance is large, and the width of microstrip line will be too wide when the characteristic impedance is small. In this case, the high-impedance characteristic of the parallel coupled microstrip line provides the possibility to design a microstrip power divider with large division ratio [12]. Figure 2 shows the structure of the coupled microstrip line with two short-circuit terminations and its equivalent circuit model [12, 13].

The coupled microstrip line can be analyzed by the even-odd mode analysis method, and the characteristic impedance of the equivalent structure can be expressed by the characteristic impedances Z_{0e} and Z_{0o} of the even mode and odd mode, respectively [12]. The even-mode and odd-mode characteristic impedances are given as follows [12]:

$$\begin{aligned} Z_{0e} &= Z_{01}\frac{C}{1-C}, \\ Z_{0o} &= Z_{01}\frac{C}{1+C}, \end{aligned} \tag{1}$$

where C is the coupling coefficient and Z_{01} is the required characteristic impedance. Once the value of C is determined, the width of coupled line w and the spacing of the coupled lines g can be easily obtained through software. In the design of this letter, the resistance value of the high-resistance line is selected to be 500 Ω.

Figure 3 shows the model and simulation results of a 500 Ω coupled microstrip line with two short-circuit ends. The results show that the high-resistance line satisfies $|S_{11}|$ <-15 dB and $|S_{21}|$ <-0.3 dB at 34–36 GHz, which has good performance in high-impedance characteristics.

2.2. Design of Divider with Large Division Ratio. In order to verify the feasibility of using the high-resistance characteristic of the coupled microstrip line to realize a large division ratio, an example of a divider with a division ratio of 12 : 1 : 1 is designed. Figure 4 shows the configuration of the divider. The 100 Ω microstrip line is divided into two high-impedance branches and one low-impedance branch, and there is a $1/4\lambda_g$ matching branch between the three-way parallel branch and the 100 Ω microstrip line for impedance matching. The two high-impedance branches of the power

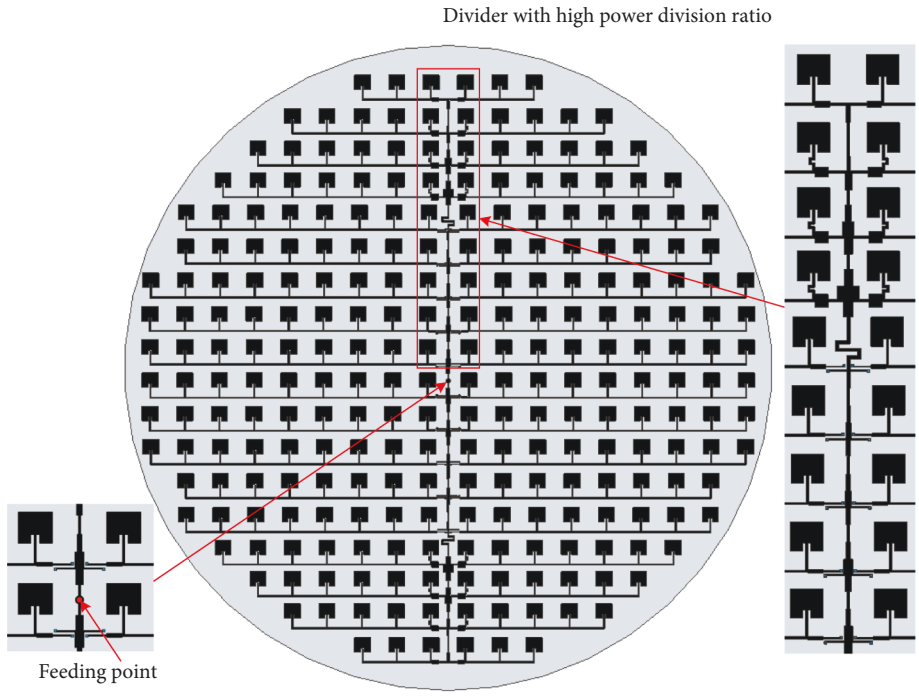

Figure 1: Configuration of the proposed antenna array.

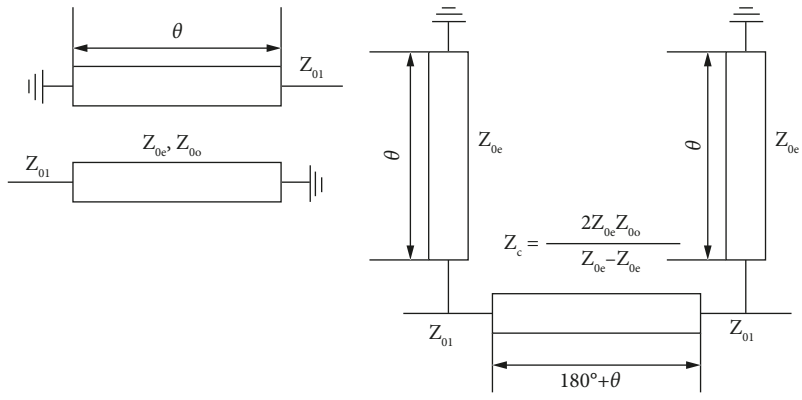

Figure 2: (a) Structure of coupled microstrip line with two shorts. (b) Equivalent circuit model.

divider are realized by using 500 Ω coupled microstrip line, and main branch uses 40.92 Ω microstrip line. Therefore, the total parallel impedance of the two parallel branches and the main branch is 500 Ω//500 Ω//40.92 Ω = 35.16 Ω, and the impedance of the $1/4\lambda_g$ matching branch is $\sqrt{35.16 \times 100}\Omega = 59.29\ \Omega$. According to simulation results, $|S_{21}|$ is about −1 dB near the 35 GHz frequency, and $|S_{31}|$ and $|S_{41}|$ are about −11.5 dB, which verifies the correctness of the theoretical design.

In order to explore the sensitivity of the power divider in Figure 4(a) to the machining accuracy, the influence of machining error on the division ratio was simulated. As shown in Figure 5(a), w is the line width of the high-resistance line, g is the distance between the high-resistance lines, and Δt is the vertical offset distance of the short-circuit ends. Figures 5(b), 6(a), and 6(b) show the variation of division ratio with offset error Δt, line width error Δw, and spacing error Δg, respectively. The simulation shows that the division effect of the divider is sensitive to the machining error, especially to the spacing error Δg. Therefore, the divider using the high-resistance line has higher requirements on the machining accuracy.

2.3. Design of Feeding Network. The feeding network with multi-stage and large division ratio is the key part of the antenna array in this design. According to the size of aperture and element arrangement of the array, the total number of array elements is determined to be 256. The number of elements in each row array starting from the center of the array to the edge of the array is 18, 18, 18, 16, 16,

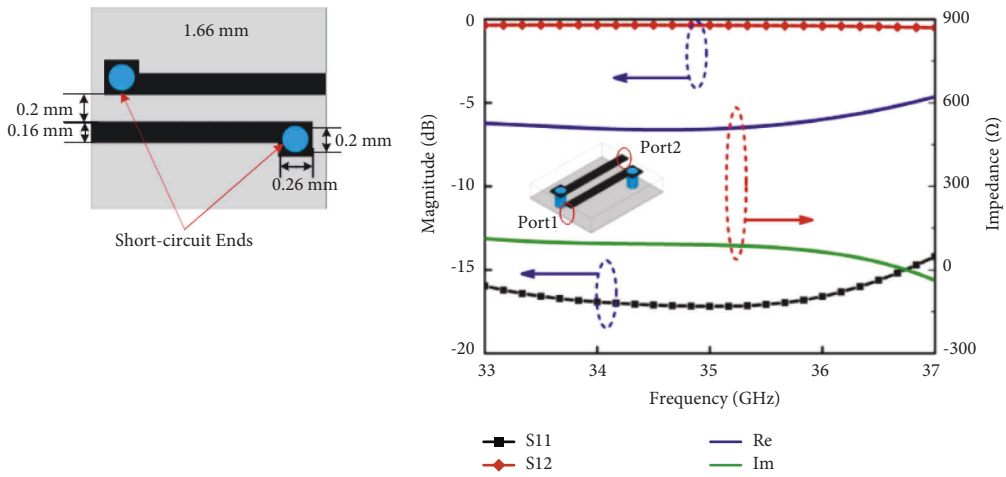

Figure 3: (a) Configuration of coupled microstrip line with two shorts. (b) Simulation results.

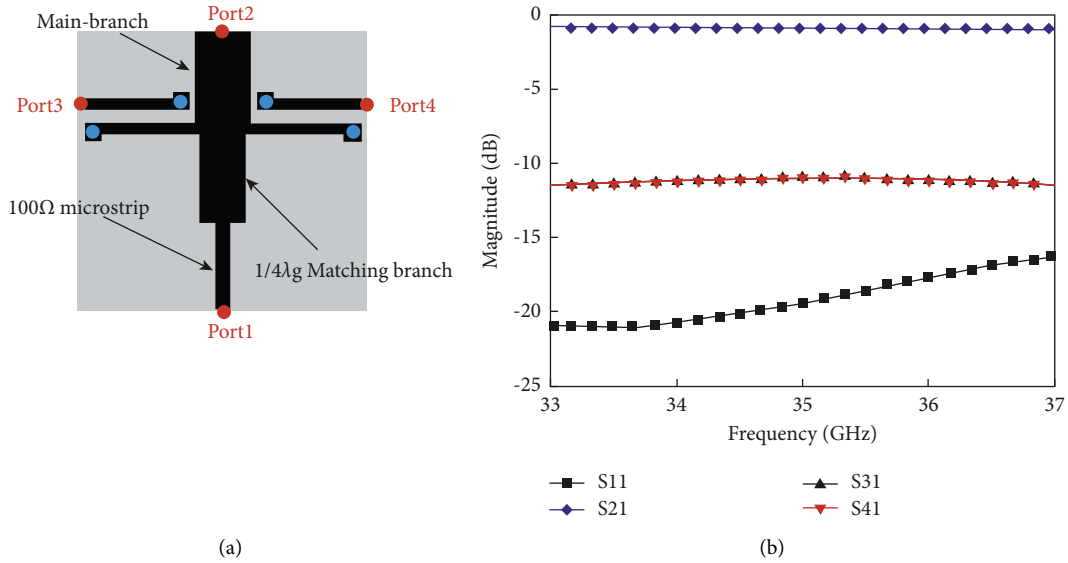

Figure 4: (a) Configuration of divider with division ratio of 12 : 1 : 1. (b) Simulation results.

14, 12, 10, and 8. In order to feed each element equally in the array, the division ratios of the main branch and two parallel branches of each stage are 12.22 : 1 : 1, 10.22 : 1 : 1, 8.22 : 1 : 1, 7.25 : 1 : 1, 5.25 : 1 : 1, 4.00 : 1 : 1, 2.67 : 1 : 1, and 1.20 : 1 : 1. Figure 7 shows the division ratio of each stage of feeding network of half array, and the label of the stage is shown in the figure.

Figure 8 shows the configuration of feeding network of half array. In order to facilitate the design, the feeding network is divided into two parts: section A and section B. The two parallel branches of each power divider adopt the high-resistance line structure and traditional microstrip structure in section A and section B, respectively. The division ratio required in section A is relatively small, which can be realized by traditional microstrip lines, and the division ratio required in section B is large, which requires the use of high-resistance lines as parallel branches to realize the large division ratios.

The resistance value of the main branch in each stage is defined as $Z_m = Z_b/r$, where Z_b is the parallel branch line impedance which is 100 Ω and 500 Ω for section A and section B, where m is the label of the divider stage and r is the power division ratio between the main branch and the two parallel branches of the corresponding stage.

Due to the different impedance of the matching branch of each stage, this will lead to different path distances of the current under the same phase change. Therefore, the distance between the parallel branches of each stage is not the same, and this distance is determined to ensure that the ends of each parallel branch can obtain the same current phase, so as to ensure that each array element in the array can obtain in-phase excitation.

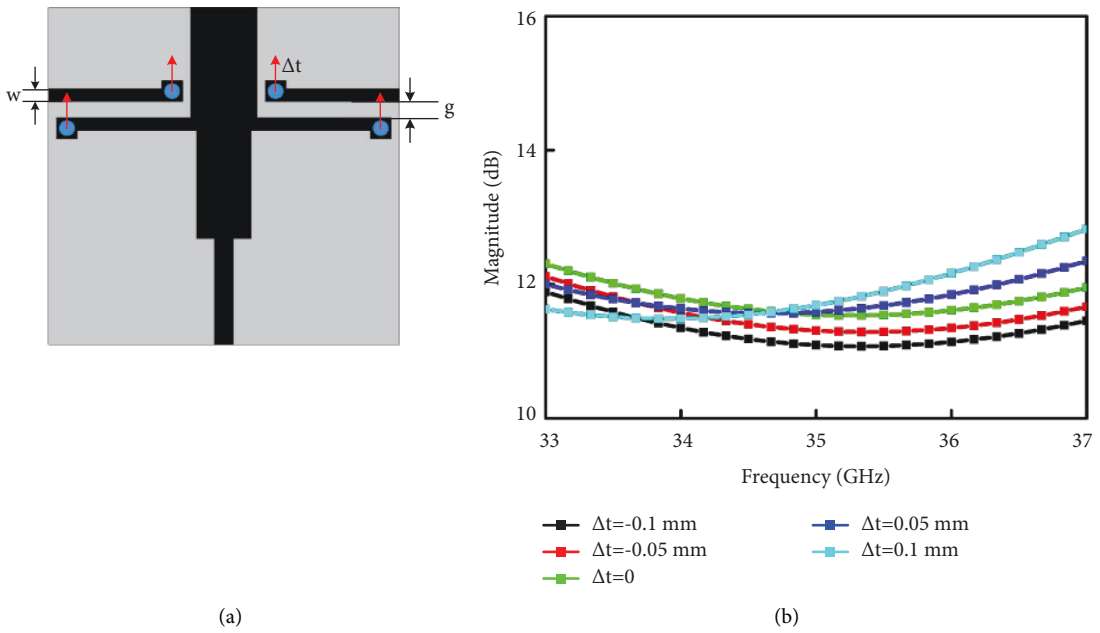

Figure 5: (a) Divider using the high-resistance line. (b) Variation of division ratio with offset error Δt.

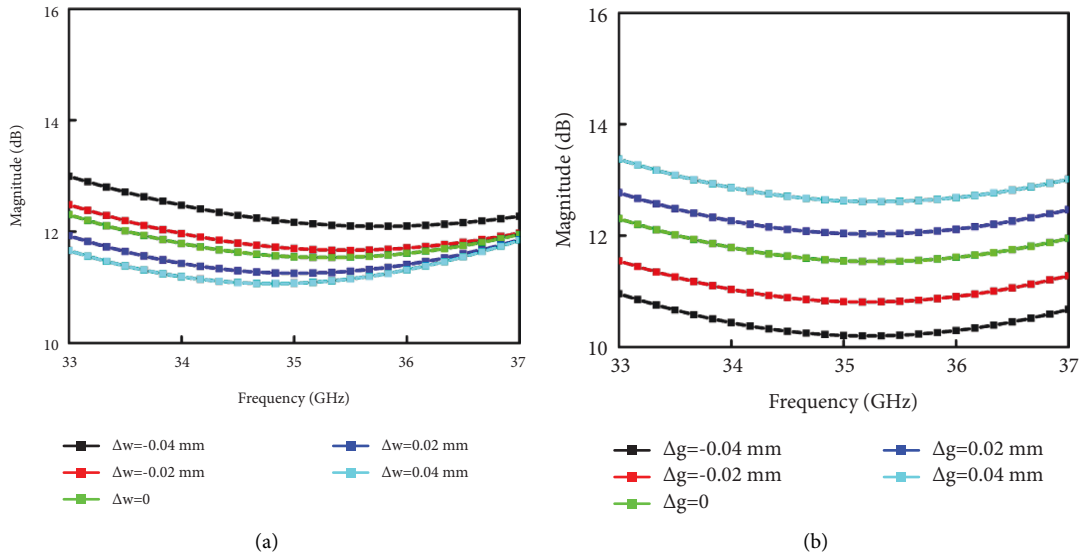

Figure 6: (a) Variation of division ratio with line width error Δw. (b) Variation of division ratio with spacing error Δg.

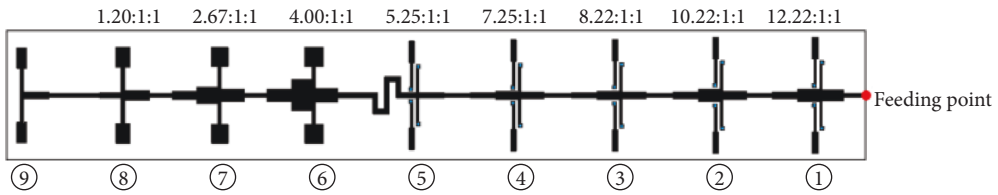

Figure 7: Division ratio of each stage of feeding network of half array.

The two parallel branches of each divider are connected to row arrays, and the distance between the array elements in row arrays is λ_g at 35 GHz. Figure 9 shows element arrangement of the row array of section A and section B respectively, and the equivalent circuit is shown in Figure 10. The series impedance network of the row array can be equivalent to parallel admittance network, each antenna element is equivalent to the admittance of

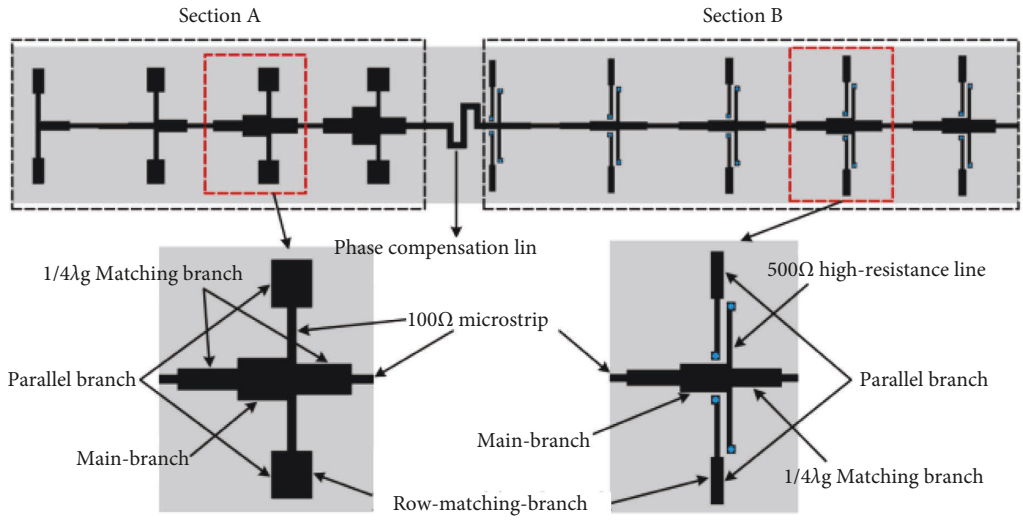

Figure 8: Configuration of feeding network of half array.

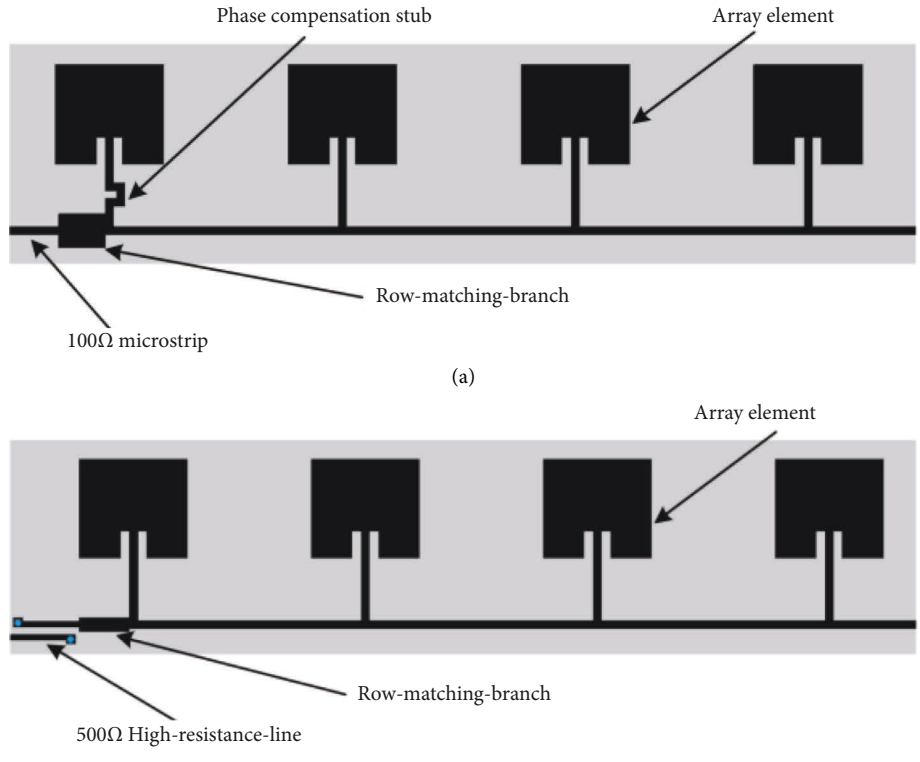

Figure 9: Element arrangement of the row array. (a) Section A. (b) Section B.

$Y_A = G + jB$, and the imaginary part of Y_A is 0 when the antenna is resonant. The input admittance of the parallel branch is Y_{in}, which is matched to 100 Ω and 500 Ω in section A and section B, respectively. Row-match-branch is used to match the parallel branch and row array, and the admittance value of row-match-branch is Y_c. Taking the number of elements of each row array as n, the input admittance at Y_c is $Y_{inc} = nY_A$, and the resistance value Z_c of row-match-branch can be calculated by the following formula:

$$Z_c = \sqrt{Z_{in} Z_{inc}}. \quad (2)$$

It is worth noting that for some row arrays, the resistance of row-match-branch is small; in this case, the microstrip line width is very wide, which will affect the current path,

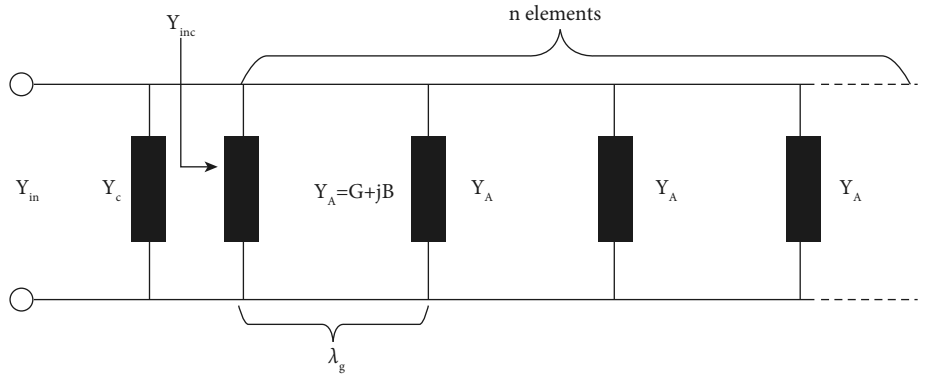

Figure 10: Equivalent circuit of row array.

Table 1: Impedance and line width of main branch and row-matching-branch of each stage of feeding network.

Stage number	1	2	3	4	5	6	7	8
Z_m (Ω)	40.9	48.9	60.8	69.0	95.2	25.0	37.5	83.3
W_m (mm)	1.05	0.82	0.58	0.47	0.26	2.02	1.19	0.34
Z_c (Ω)	74.5	74.5	74.5	79.1	79.1	37.8	40.8	44.7
W_c (mm)	0.38	0.38	0.38	0.34	0.34	1.18	1.06	0.64

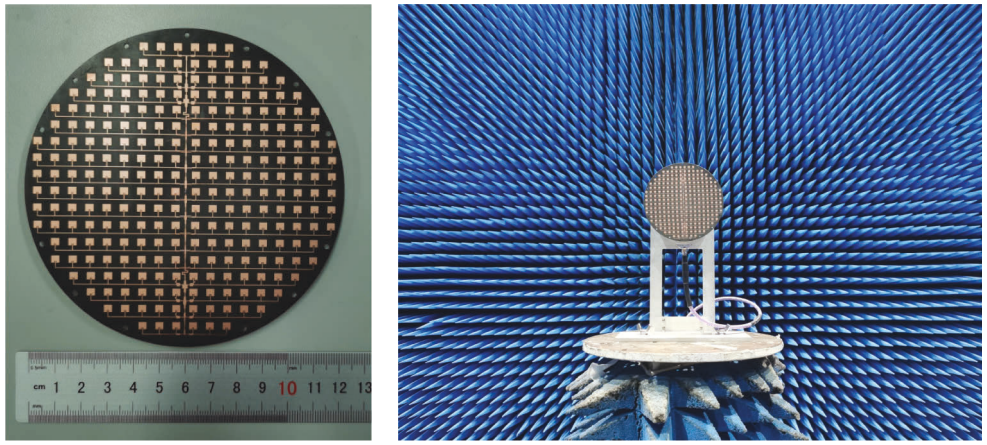

(a) (b)

Figure 11: Element arrangement of the row array. (a) Photograph of the fabricated antenna. (b) Photograph of the antenna tested in the anechoic chamber.

and it will make the current phase of the element nearest to row-match-branch to be advanced. Therefore, the phase compensation stub is added for the first array element adjacent to row-match-branch.

After calculation, Table 1 lists impedance value and line width of main branch and row-matching-branch of each stage of feeding network, where W_m and W_c are the line widths of the main branch and row-matching-branch, respectively.

3. Prototype Fabrication and Measurement

A 256-element array antenna at 35 GHz is fabricated and measured. Figure 11(a) shows a photograph of the fabricated antenna, and Figure 11(b) shows a photograph of the antenna tested in the anechoic chamber. The measured results of reflection coefficient and gain of the proposed antenna are shown in Figure 12. Figure 13 shows the measured radiation efficiency and aperture efficiency. It can be seen that the measured bandwidth of the antenna array is 34 GHz to 35.6 GHz within $|S_{11}| < -10$ dB. The difference between the simulated and the measured $|S_{11}|$ is mainly due to the error of the machining accuracy and the loss of the microstrip structure, and the machining error of the metal vias of the coupling line will significantly affect the impedance matching of the divider, which will result in the difference between the simulation and the measured results. The maximum simulated gain of the antenna is 31.6 dBi at 35 GHz, and maximum measured gain is 29.5 dBi at 35 GHz, which correspond to the measured radiation efficiency and

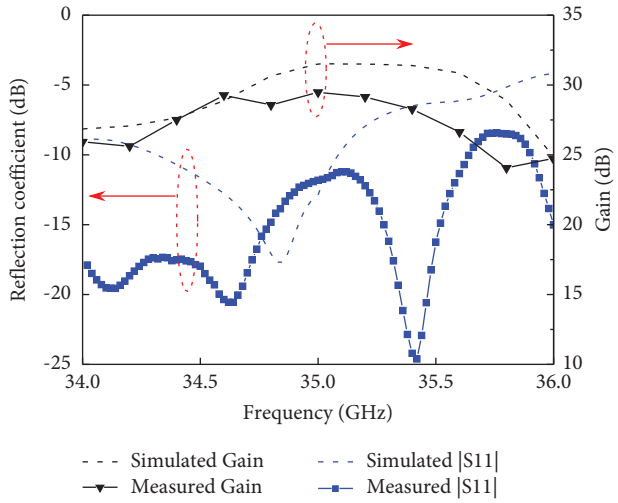

Figure 12: Simulated and measured results of reflection coefficient and gain.

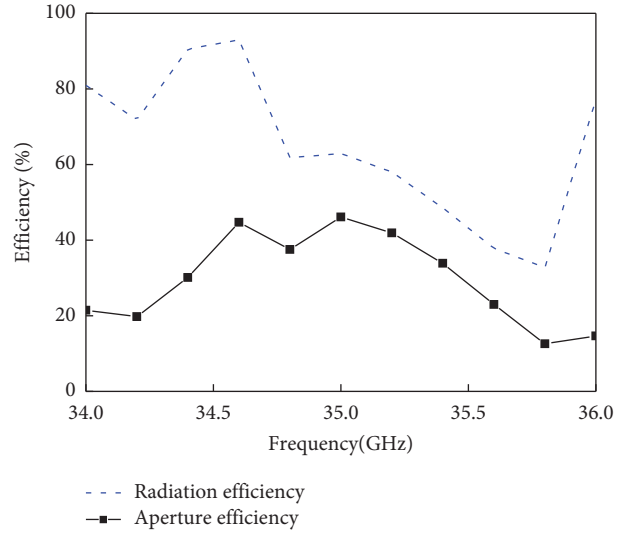

Figure 13: Measured radiation efficiency and aperture efficiency.

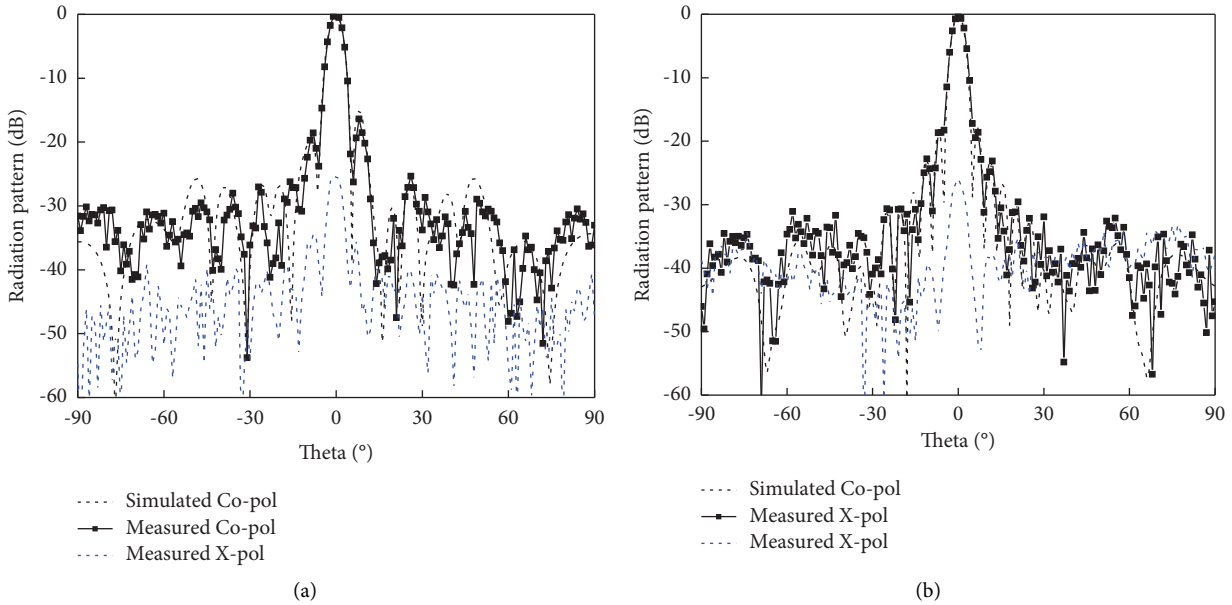

Figure 14: Normalized radiation patterns at 35 GHz. (a) E-plane. (b) H-plane.

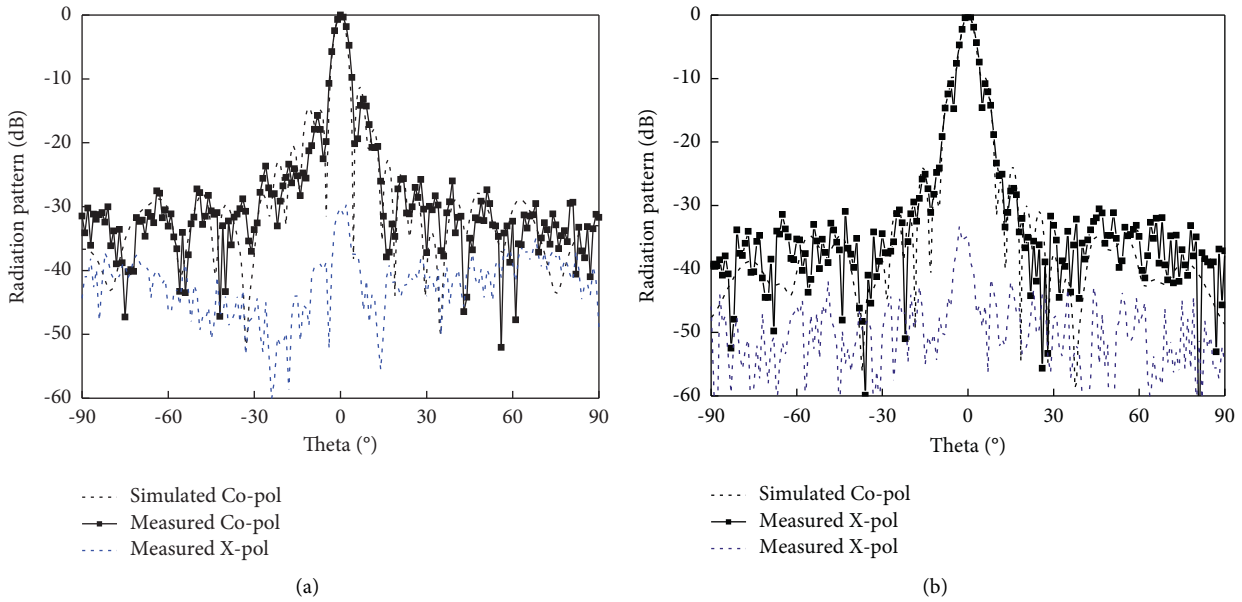

Figure 15: Normalized radiation patterns at 34.6 GHz. (a) E-plane. (b) H-plane.

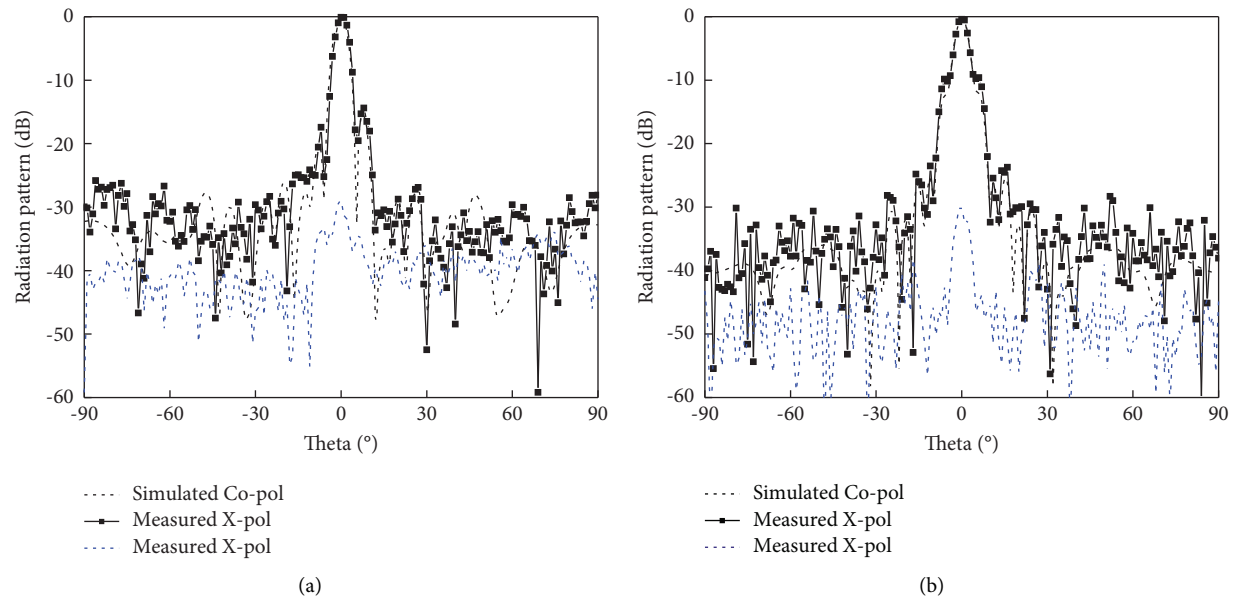

Figure 16: Normalized radiation patterns at 35.4 GHz. (a) E-plane. (b) H-plane.

measured aperture efficiency of 61.66% and 46.07%, respectively. The measured cross polarization of the antenna is less than −25 dB. Figure 14 shows normalized radiation patterns of the antenna at 35 GHz, and the side lobes on the E-plane and H-plane are −15.0 dB and −17.9 dBi, respectively. Figures 15 and 16 show the radiation patterns of the antenna at 34.6 GHz and 35.4 GHz, respectively. As the frequency shifts, the SLL of the H-plane increases, and the pattern gradually deteriorates.

It can be seen from the radiation pattern of the E-plane of the antenna that the SLL of is unbalanced; this is because even if the structure of the multi-stage divider is centrally symmetric and the designed division ratio is ideal, the arrangement of the array elements in the direction of the E-plane is not symmetrical with the feeding point, and the coupling relationship between the array elements and the row feeding line in the E-plane direction is also asymmetric. The influence of these asymmetric factors causes the impedances at two sides of the feeding point to be unequal, which causes the energy distributed in the direction of the E-plane to become unbalanced and finally leads to an unbalanced SLL of the E-plane beam. At the same time, the machining error makes this result even more serious.

The coupling between the array elements is very important for the antenna design. In this paper, no decoupling design is included, and the element is simulated by the

Table 2: Comparison with other reported planar array antennas.

Ref.	f_0 (GHz)	Max gain (dBi)	Number of elements	Impedance bandwidth (%)	Aperture size	Radiation/ aperture efficiency (%)	Configuration	Feeding mechanism	Circular aperture design	Design complexity
[2]	14.25	24.5	256	5.6	$13.3\lambda_0 \times 12.35\lambda_0$	20/N.A.	Single-layer PCB	Microstrip feeding	Not suitable	Easy
[6]	37.5	24	64	16	$6.4\lambda_0 \times 6.4\lambda_0$	41.6/N.A.	3-layer PCB + air gap	PRGW feeding	Not suitable	Difficult
[5]	34	17.4	16	35.5	$\sim 5.25\lambda_0 \times 5.25\lambda_0$	N.A./25	3-layer PCB	SIGW feeding	Not suitable	Difficult
[8]	28	21.8	42	6.3	N.A.	N.A./21.2	2-layer PCB	SIW feeding	Not suitable	Easy
This work	35	29.5	256	4.6	$\pi \times 7\lambda_0 \times 7\lambda_0$	61.66/46.07	Single-layer PCB	Microstrip feeding	Suitable	Difficult

periodic boundary of the HFSS software during the design, which makes the influence of mutual coupling between elements taken into account. However, [14, 15] provide good method for future work.

Table 2 lists the comparison with other reported planar array antennas. The fabrication cost mainly depends on the number of layers and materials of the antenna. Design complexity is based on the number of parameters required to design the entire antenna and the number of layers of the antenna. The antennas in reference [2, 8] only need 10~20 parameters and 1~2 layers, and the design difficulty is relatively easy. The antennas in reference [5, 6] need 30~40 parameters and multilayer structure, which is more difficult to design. Although the proposed antenna is single-layer structure, there are a total of 78 parameters required for the design; therefore, the antenna also has high design complexity. Compared with the antennas in other references, although the antenna in this paper has the advantages of high efficiency, low cost, and single layer, it also has the disadvantage of complex design.

4. Conclusion

In this paper, a single-layer circular aperture high-efficiency microstrip array antenna that works in *Ka* band is presented. By using the high-impedance characteristic of the coupled microstrip line, a novel multi-stage feeding network that can realize large division ratio is proposed, which can be used to design large-scale series-fed microstrip array and obtain high efficiency. According to the proposed theory, an antenna prototype was designed, we fabricated and tested the designed antenna, and the results show that the maximum gain is 29.5 dBi at 35 GHz, which correspond to the radiation efficiency and aperture efficiency of 61.66% and 46.07%, respectively, and the impedance bandwidth of the antenna array is 34 GHz to 35.6 GHz within $|S_{11}| < -10$ dB. In summary, the proposed antenna array has the advantages of high efficiency, single layer, and low cost, which is an excellent candidate for millimeter-wave large-scale circular aperture array application [16–22].

Data Availability

No data were used to support this study.

Conflicts of Interest

The authors declare that they have no conflicts of interest.

References

[1] X. Zeng, K. Huang, Z. Hu, Q. Chen, and W. Xiao, "A circularly polarized HTS microstrip antenna array with controllable cryostat," *International Journal of Antennas and Propagation*, vol. 20176 pages, Article ID 6035202, 2017.

[2] H. Wang, D. G. Fang, and X. G. Chen, "A compact single layer monopulse microstrip antenna array," *IEEE Transactions on Antennas and Propagation*, vol. 54, no. 2, pp. 503–509, Feb. 2006.

[3] M. Wang, D.-Yu Wang, W. Wu, and Da-G. Fang, "Single-layer, dual-port, dual-band, and orthogonal-circularly polarized microstrip antenna array with low frequency ratio," *Wireless Communications and Mobile Computing*, vol. 2018, p. 1, Article ID 5391245, 2018.

[4] Y. Li and K. M. Luk, "60-GHz substrate integrated waveguide fed cavity-backed aperture-coupled microstrip patch antenna arrays," *IEEE Transactions on Antennas and Propagation*, vol. 63, no. 3, pp. 1075–1085, March 2015.

[5] T. Li and Z. N. Chen, "Wideband sidelobe-level reduced Ka -band metasurface antenna array fed by substrate-integrated gap waveguide using characteristic mode analysis," *IEEE Transactions on Antennas and Propagation*, vol. 68, no. 3, pp. 1356–1365, March 2020.

[6] X. Jiang, F. Jia, Y. Cao et al., "Ka-band 8 × 8 low-sidelobe slot antenna array using a 1-to-64 high-efficiency network designed by new printed RGW technology," *IEEE Antennas and Wireless Propagation Letters*, vol. 18, no. 6, pp. 1248–1252, June 2019.

[7] H. Khalili, K. Mohammadpour-Aghdam, S. Alamdar, and M. Mohammad-Taheri, "Low-cost series-fed microstrip antenna arrays with extremely low sidelobe levels," *IEEE Transactions on Antennas and Propagation*, vol. 66, no. 9, pp. 4606–4612, Sept. 2018.

[8] P. A. Dzagbletey and Y.-B. Jung, "Stacked microstrip linear array for millimeter-wave 5G baseband communication," *IEEE Antennas and Wireless Propagation Letters*, vol. 17, no. 5, pp. 780–783, May 2018.

[9] S. Sugawa, K. Sakakibara, N. Kikuma, and H. Hirayama, "Low-sidelobe design of microstrip comb-line antennas using stub-integrated radiating elements in the millimeter-wave

band," *IEEE Transactions on Antennas and Propagation*, vol. 60, no. 10, pp. 4699–4709, 2012.

[10] Z. Shaterian, A. K. Horestani, and J. Rashed-Mohassel, "Design of slot array antenna in groove Gap waveguide technology," *IET Microwaves, Antennas & Propagation*, vol. 13, no. 8, pp. 1235–1239, 2019.

[11] A. Khaleghi, Z. TalePour, and M. Ramazan, "Resonant slot antenna array on a ridge gap waveguide," *IET Microwaves, Antennas & Propagation*, vol. 11, no. 8, pp. 1092–1097, 2017.

[12] B. Li, X. Wu, and W. Wu, "A 10:1 unequal wilkinson power divider using coupled lines with two shorts," *IEEE Microwave and Wireless Components Letters*, vol. 19, no. 12, pp. 789–791, 2009.

[13] H.-R. Ahn, K. Min, D. Kang, S. Hong, and B. Kim, "Coupling-compensated 180 phase shift coupled-line filters terminated in arbitrary impedances," in *Proceeding of the APMC Proceedings*, pp. 649–652, Yokohama, Japan, December 2006.

[14] M. Alibakhshikenari, B. S. Virdee, P. Shukla et al., "Impedance bandwidth improvement of a planar antenna based on metamaterial-inspired T-matching network," *IEEE Access*, vol. 9, pp. 67916–67927, 2021.

[15] M. Alibakhshikenari, M. Khalily, B. S. Virdee, C. H. See, R. A. Abd-Alhameed, and E. Limiti, "Mutual coupling suppression between two closely placed microstrip patches using EM-bandgap metamaterial fractal loading," *IEEE Access*, vol. 7, pp. 23606–23614, 2019.

[16] I. Slomian, S. Gruszczynski, and K. Wincza, "Symmetrical series-fed dual-polarised microstrip antenna lattice with odd number of radiating elements," *IET Microwaves, Antennas & Propagation*, vol. 10, no. 7, pp. 701–708, 2016.

[17] K. Wincza and S. Gruszczynski, "Microstrip antenna arrays fed by a series-parallel slot-coupled feeding network," *IEEE Antennas and Wireless Propagation Letters*, vol. 10, pp. 991–994, 2011.

[18] T. Li, H. Meng, and W. Dou, "Design and implementation of dual-frequency dual-polarization slotted waveguide antenna array for ka-band Application," *IEEE Antennas and Wireless Propagation Letters*, vol. 13, pp. 1317–1320, 2014.

[19] M. Ferrando-Rocher, J. I. Herranz-Herruzo, A. Valero-Nogueira, and B. Bernardo-Clemente, "Full-metal K-Ka dual-band shared-aperture array antenna fed by combined ridge-groove gap waveguide," *IEEE Antennas and Wireless Propagation Letters*, vol. 18, no. 7, pp. 1463–1467, July 2019.

[20] M. Alibakhshikenari, F. Babaeian, B. S. Virdee et al., "A comprehensive survey on "various decoupling mechanisms with focus on metamaterial and metasurface principles applicable to SAR and MIMO antenna systems"," *IEEE Access*, vol. 8, pp. 192965–193004, 2020.

[21] H. Kumar and G. Kumar, "Broadband monopulse microstrip antenna array for X-band monopulse tracking," *IET Microwaves, Antennas & Propagation*, vol. 12, no. 13, pp. 2109–2114, 2018.

[22] H.-C. Chen, T. Chiu, and C.-L. Hsu, "Design of series-fed bandwidth-enhanced microstrip antenna array for millimetre-wave beamforming applications," *International Journal of Antennas and Propagation*, vol. 201910 pages, Article ID 3857964, 2019.